Intricate relationship between pressure-induced electronic and structural transformations in $FeCr_2S_4$

Y. Amiel,[1] G. Kh. Rozenberg,[1] N. Nissim,[1] A. Milner,[1] M. P. Pasternak,[1,*] M. Hanfland,[2] and R. D. Taylor[3]

[1]*School of Physics and Astronomy, Tel-Aviv University, Ramat-Aviv 69978, Tel-Aviv, Israel*

[2]*European Synchrotron Radiation Facility, BP 220, 38043 Grenoble Cedex, France*

[3]*MST-10, MS-K764, Los Alamos National Laboratory, Los Alamos, New Mexico 87545, USA*

(Received 26 July 2011; revised manuscript received 30 October 2011; published 22 December 2011)

Electrical-transport, magnetic and structural properties of the ferrimagnetic semiconductor $FeCr_2S_4$ (T_N = 170 K) have been studied by electrical resistance, $R(P, T)$, ^{57}Fe Mössbauer spectroscopy (MS), and synchrotron x-ray diffraction to 20 GPa using diamond anvil cells. It was found that the local maximum, $R_{max}(P)$ on the $R(T)$ curve, corresponding to the colossal magnetoresistance effect, is substantially reduced and broadened with pressure increase accompanied by a shift to higher temperatures and finally disappears at ∼7 GPa, the highest pressure of the single, high-spin spinel phase designated as LP1. Suppression of $R_{max}(P)$ precedes a gap closure leading to metallization at ∼7 GPa. The 7–10 GPa range is a coexistence pressure zone composed of three phases: (i) LP1, a paramagnetic spinel (SG $Fd3m$); (ii) LP2, a nonmagnetic isostructural spinel; and (iii) HP1, a high-spin Cr_3S_4 (SG $I2/m$) type structure. Based on MS and $R(P, T)$ studies it was concluded that the Mott transition is responsible for the onset of metallization (correlation breakdown) coinciding with the collapse of Fe^{2+} moments. The shortening of the Fe-O bond length due to the electronic transition leads to a volume decrease of the low pressure (LP) phase by ∼1%. This electronic transition initiates a structural instability of the spinel structure resulting in a first-order phase transition into HP1, a post-spinel with Cr_3S_4-like structure. The onset of HP1 is accompanied by the Fe^{2+} 4 → 6 coordination number increase resulting in an additional ∼12% volume reduction. In the coexistence zone the post-spinel phase is paramagnetic, but at $P > 10$ GPa an isostructural transition takes place and Fe^{2+} becomes nonmagnetic, as evidenced from the large drop of the isomer shift and of the quadrupole splitting. The structural transition is irreversible with the isothermal pressure decrease, and the Cr_3S_4-like structure remains upon full release of pressure at 300 K. Interestingly at decompression the high pressure (HP) phase undergoes a reverse noncorrelated → correlated transition recovering its localization features, e.g., insulating state and paramagnetism with $T_N \leqslant 6$ K. The original room temperature (RT), LP spinel phase is finally recovered following heat treatment at 400 °C.

DOI: 10.1103/PhysRevB.84.224114 PACS number(s): 81.40.Vw, 72.80.Ga, 76.80.+y, 75.30.Kz

I. INTRODUCTION

$FeCr_2S_4$ (Daubréelite) attracted attention during the 1960's and 1970's due to being both a ferrimagnet and a semiconductor.[1] Around the Néel temperature (T_N = 200 K) this material exhibits a magnetoresistance effect: the resistivity vs temperature dependence shows a well-pronounced peak that flattens upon the application of a magnetic field.[2] In 1997 Ramirez *et al.*[3] brought back the attention of this material with the notion that its magnetoresistance effect is a reminiscent of the famous colossal magnetoresistance (CMR) of the manganites.[4] And indeed many of the basic features of manganites may be present in $FeCr_2S_4$, although with a different flavor, namely, strong coupling between the spins of the charge carriers and the static magnetic moments,[5] spin-polarized band structure at the Fermi level,[6] and a signature of a small-polaron conductivity mechanism.[7] All these features motivated our present studies in which pressure has been added as an additional thermodynamic probe.

Similar to other Mott insulators, the localization of carriers, and consequently the insulating behavior of $FeCr_2S_4$, is a result of strong on-site Coulomb repulsion that opens an energy gap within the 3d band.[8] The magnetic state of such materials is intimately linked to the transition-metal ion electronic state, and their electrical/magnetic properties can be substantially altered by chemical doping or application of pressure, culminating in an insulator-metal (IM) transition concurrent with the collapse of local moments,[9] the so-called Mott transition. An attempt to study the effect of pressure on the magnetic and electronic properties of $FeCr_2S_4$ had been performed by Tsurkan *et al.*[10] They found that with applied pressure there is a linear increase in T_N and in the temperature of the resistance peak R_{max} associated with the CMR effect. However, these studies, as most other studies of electronic properties of CMR materials, were limited to the low pressure range ($P \leqslant 2$ GPa), which does not produce a sufficient energy density to initiate the Mott transition.

It is noteworthy that the Mott transition phenomena in various Fe-based oxides were studied rather extensively under pressure (Ref. 11 and references therein). Because of the high degree of the Fe-S covalence-bonding nature which leads to a smaller correlation Mott-Hubbard gap compared to the Fe-oxides, it is expected that a pressure-induced Mott transition may occur at relatively lower pressure. And indeed, studies carried out with FeS[12] revealed that the IM transition is a Mott transition, coinciding with the collapse of the Fe^{2+} moments at ∼6 GPa

At ambient conditions $FeCr_2S_4$ crystallizes in the normal spinel cubic structure, AB_2O_4, with space group $Fd\bar{3}m$ and $Z = 8$,[13] where the Cr^{3+} ions occupy the octahedral B and the Fe^{2+} ions the tetrahedral A sites.[14] The effect of pressure on the crystal structure of $FeCr_2S_4$ was studied in the 1960's, but the emerged picture was not conclusive. Albers and Rooymans[15]

revealed a high pressure, high temperature ($P = 20$ GPa, $T = 700$ K) polymorph of $FeCr_2S_4$ reported as the NiAs-type structure (space group $P6_3/mmc$), implying a complete disorder of the $Cr^{3+}$and Fe^{2+}. On the other hand, Bouchard[16] reported a Cr_3S_4-like structure ($I2/m$), which implies strict order of the Cr occupancy in the octahedral sites.[17] Recent studies[18,19] also revealed a possible transition to a CdI_2-like structure ($P\bar{3}m1$).

In this paper we present a detailed high pressure study of the electrical-transport, magnetic, and crystallographic properties of $FeCr_2S_4$. This was carried out by combining electrical resistance, Mössbauer spectroscopy (MS), and synchrotron x-ray diffraction (XRD) to pressures of ∼20 GPa.

II. EXPERIMENTAL

The $FeCr_2S_4$ sample was synthesized by a direct solid-solid reaction of stoichiometric amounts of spectroscopically pure iron and chromium metals and sulfur in an evacuated quartz tube and heated in steps to 800 and then to 1000 °C. For MS measurements the Fe content was enriched to 25% with ^{57}Fe. The sample quality and integrity was checked by XRD and MS. Pressure was generated using miniature opposing-plates diamond anvil cells (DACs)[20] for MS and $R(P, T)$ studies and membrane driven cells for XRD studies. Anvils with 300-, 500-, and 700-μm diameter culet sizes were used. Samples were loaded into cavities of 100, 200, or 300 μm in diameter, respectively, and 30–40-μm height cavities drilled in 301-SS or Rhenium gaskets.

XRD studies were performed up to 20 GPa in the angle-dispersive mode at the ID9 beam-line of the European Synchrotron Radiation Facility, Grenoble. Two series of measurements were performed: (i) at $\lambda = 0.3738$ and (ii) at 0.4167 Å wavelengths. Diffraction images were collected using image plates with exposure times of ∼5 sec. The image data were integrated using the FIT2D program[21,22] and the resulting diffraction patterns were analyzed by Rietveld refinement using the GSAS[23] and EXPGUI[24] software packages. Pressure was measured using the ruby fluorescence technique and Au markers. Nitrogen or helium was used as pressure medium.

Electrical studies. Four-probe DC resistance measurements were carried out up to 10 GPa with 5-μm-thick Pt-foil electrodes placed on the truncated culet of one of the anvils insulated from the metallic gasket by a mixture layer of Al_2O_3/NaCl combined with epoxy. The pressure gradient in the region between contacts overlapping the sample area during resistance study was typically 5–10%. The $R(T)$ measurements were carried out in the range 4.2–300 K using a dip-stick sample holder immersed in helium vapor inside a LHe storage Dewar.[25] Sample temperatures were determined using an attached Si-diode thermometer.

Mössbauer measurements were carried out with a top-loaded LHe cryostat using a ^{57}Co(Rh) point source in the 5–300 K temperature range and up to ∼20 GPa. Spectra were analyzed using proper spin-Hamiltonian fitting programs from which the following hyperfine interaction parameters were derived: (i) the quadrupole splitting QS and the magnetic hyperfine field H_{hf}; (ii) the isomer shift (IS), which is proportional to the s-electron density $\rho_s(0)$ at the Fe nucleus; and (iii) the respective relative abundances of the components. Nitrogen was used as a pressure medium.

Pressure was determined using Ruby fluorescence in MS and $R(P, T)$ studies.

III. RESULTS

A. Compression cycle

1. Electrical resistance

Pressure and temperature dependence of the resistance is shown in Fig. 1. The measurements were carried out only at compression. At the 0 to 5 GPa range, $R(P, T)$ reveals a local maximum R_{max} with T_{max} close to T_N (Ref. 3) and preceded by a minimum extending from 135 to 145 K. The $R_{max}(P, T)$ peak is substantially broadened with pressure increase and shifts to higher temperature. Most of the T_{max}-shift occurs at $P >$ 3 GPa.

The log $R(P, 77\ K)$ and log $R(P, 296\ K)$ corresponding to the ordered (ferrimagnetic) and paramagnetic states, respectively, decrease linearly with different slopes and intersect at ∼6.8 GPa [see Fig. 2(a)]. The slope obtained from least squares fitting results in $d(\ln R)/dP$: −0.39 (GPa^{-1}) and −0.24 GPa^{-1} for 77 K and 296 K, respectively. At $P \sim 7$ GPa an abrupt resistance drop of almost two orders of magnitude takes place (Fig. 1), suggestive of an onset of metallization. And indeed the $R_P(T)$ measurements clearly show a change in sign of the resistance derivative dR/dT, namely from a gapped (negative) to a metal system behavior (positive). At 7 GPa the negative slope of the $R(T)$ curve is reduced and at $T >$ 100 K it becomes positive. As will be shown from the MS data, at 7 GPa the sample consists of a mixture of the LP1 (gapped) and LP2 (metallic) phase clusters but with further pressure

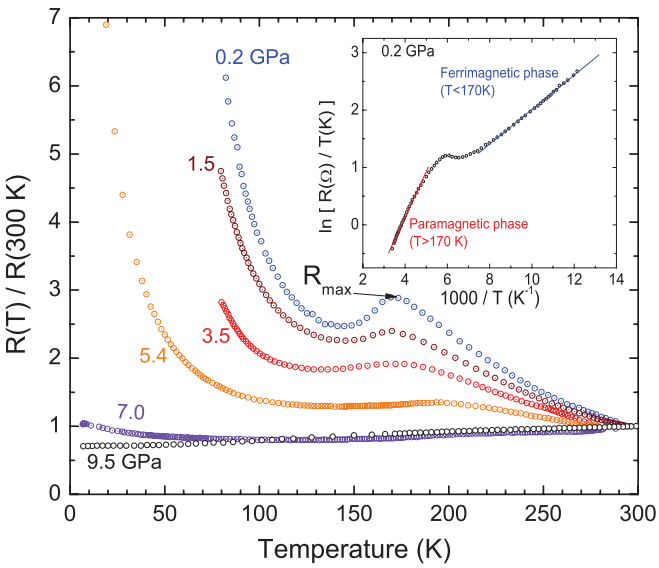

FIG. 1. (Color online) The normalized temperature dependence of the resistance at various pressures: at $P \sim 7$ GPa, the slope of the $R(T)$ curve becomes positive, signaling the onset of metallization. The inset shows the curve at $P = 0.2$ GPa of $\ln(R/T)$ vs $1000/T$ at the paramagnetic and magnetic regimes, used for obtaining the charge carrier activation energies.

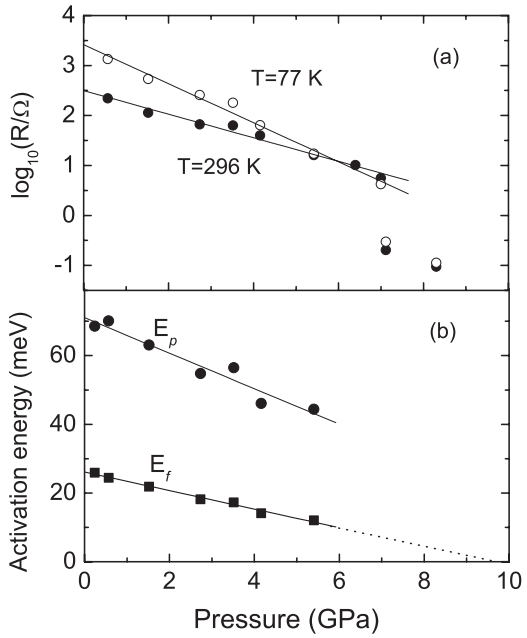

FIG. 2. (a) Pressure dependence of the logarithm of the resistance recorded at 296 and 77 K (solid and open circles, respectively). Up to 7 GPa the low-pressure phase of $FeCr_2S_4$ is a semiconductor whose gap decreases gradually with pressure. Above 7 GPa a discontinuous decrease in $R(P)$ takes place coinciding with the onset of metallization. (b) The pressure dependence of the electrical transport activation energies in the ferrimagnetic (E_f) and paramagnetic (E_p) phases, respectively. Note that the E_p values are a rough estimate.

increase the slope becomes positive over the entire temperature range (4 K–300 K).

At the ferrimagnetic phase ($T \leqslant 120$ K) the resistance data fairly well obey the relation $\log(R(P,T))/R_0 = E_f(P)/k_BT$, where k_B is the Boltzmann constant and E_f the electrical transport activation energy. $E_f(P)$ decreases linearly with pressure and a least squares fitting to the curve resulted in $dE_f(P)/dP = -2.7 \pm 0.1$ meV/GPa and $E_f(0) = 26.1 \pm 0.4$ meV [Fig. 2(a)]. The ambient pressure value agrees very well with the value measured by Wang *et al.*[7] and Yang *et al.*,[26] namely, $E_f(0) = 28.5$ and 26 meV, respectively. By extrapolation we estimated that this gap is expected to close at 9.7 ± 0.5 GPa. At the paramagnetic phase [Fig. 2(b)] the best approximation for $R(T)$ data is consistent with the relation $\log(R_n(P)/T) = E_{pol}/k_BT$, $R_n(P) = R(P)/R_0$, which is commonly associated with the small polaron hopping mechanism (see Ref. 7).

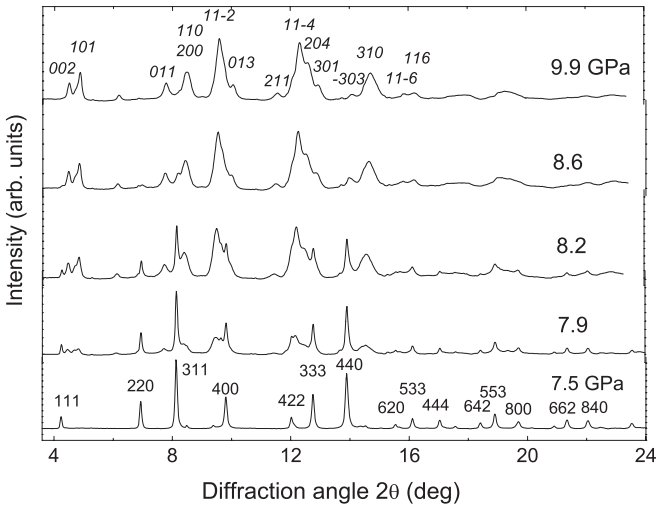

FIG. 3. X-ray powder-diffraction patterns of $FeCr_2S_4$ (background subtracted) at $T = 298$ K for various pressures. Note the appearance of the pattern of the HP phase (Cr_3S_4-like structure) at $P = 7.9$ GPa, especially the (101), (110), (11-2), (11-4), (310), etc. Italics correspond to the diffraction peaks of the HP phase.

2. *X-ray diffraction*

X-ray diffraction studies were performed at room temperature (RT) at pressures to 20 GPa. Diffraction patterns recorded in this pressure range are shown in Fig. 3.

The low pressure phase (LP). Up to 7.5 GPa, the diffraction patterns could be satisfactorily fitted with a cubic normal spinel structure, space group $Fd\bar{3}m$ (Fig. 4), resulting in $\chi^2 \leqslant 0.08$, $w_{Rp} \leqslant 0.7\%$, and Rp $< 0.4\%$. The setting commonly used[13] is with an inversion center at the origin, the tetrahedral cation at (1/8, 1/8, 1/8) and the octahedral cation at (1/2, 1/2, 1/2). The sulfur parameter in this setting is at u, u, u ($u \cong 0.75$). The lattice parameter a and the volume V decrease continuously by 2.5% and 7.3%, respectively, at this pressure range (see Fig. 5); the sulfur coordinate u is nearly constant varying between 0.738(1) and 0.739(1).

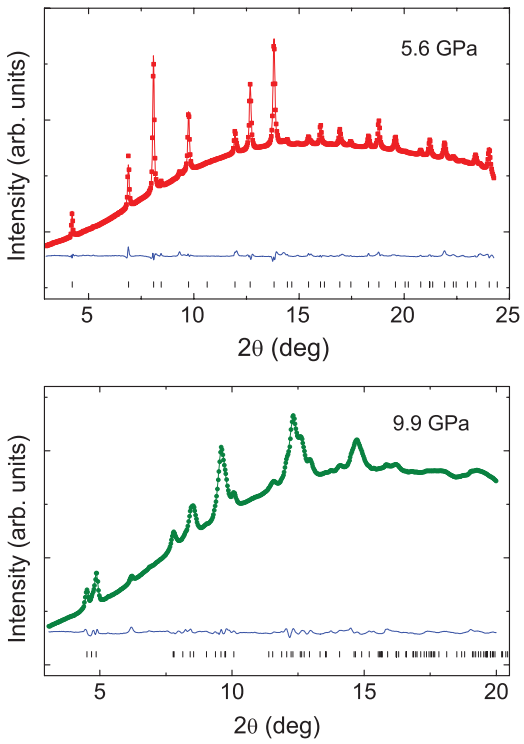

FIG. 4. (Color online) Typical examples of analyzed integrated patterns obtained for the two observed phases of $FeCr_2S_4$. The 5.6 GPa spectrum corresponds to the LP phase with $Fd\bar{3}m$ symmetry, extending from ambient pressure to 8 GPa. Above 9 GPa and at the decompression the symmetry group is $I2/m$. The GSAS program package was used.

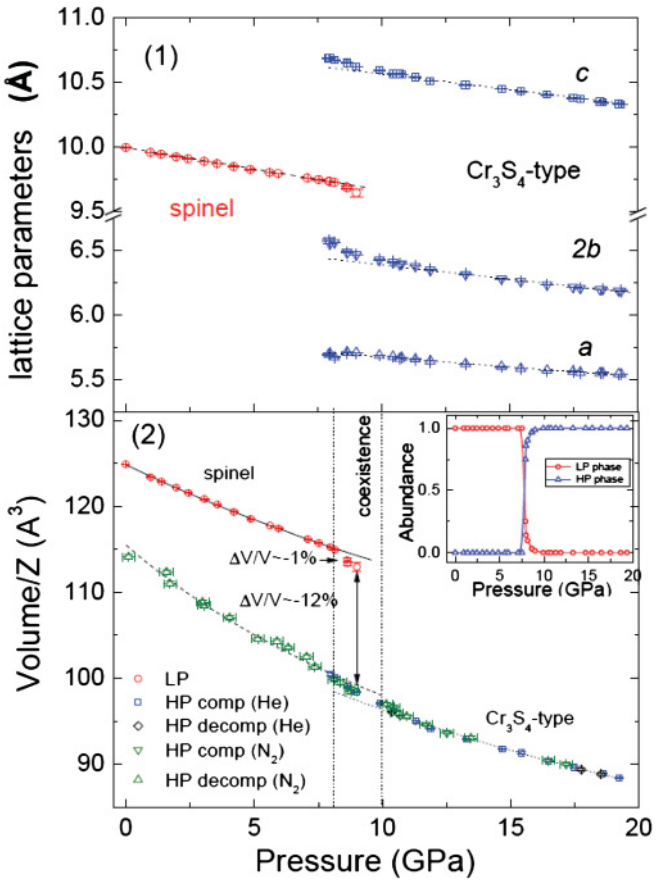

FIG. 5. (Color online) (1, upper portion) Pressure evolution of the lattice parameters of $FeCr_2S_4$ obtained at the compression cycle was with the sample using helium pressure medium. (2, lower portion) Pressure dependence of the unit cell volume. Open circles correspond to the low pressure spinel phase, ∇ and □ correspond to the brezinaite phase using nitrogen and helium pressure medium, respectively. Symbols Δ and ◇ correspond to the decompression cycle. Error bars derived from the GSAS-fitting output and multiplied by a factor of 3, as proposed by W.I.F. David.[43] With helium pressure medium the pressure uncertainties are ∼0.1 GPa. The solid, dashed, and dotted lines are the theoretical fit for the LP, HP1, and HP2 phases, respectively, using the second-order Birch-Murnaghan EOS.[28] The bulk modulus values are 85.4(6) GPa, 53.7(1.1) GPa, and 43.6(2.0) GPa for the LP, HP1, and HP2 ranges, accordingly. The volume was normalized to one unit formula of $FeCr_2S_4$, i.e., $Z = 8$ for spinel and $Z = 2$ for Cr_3S_4. The inset shows the relative abundance of the LP and HP phases obtained from XRD as a function of pressure.

The high pressure phase (HP). At $P \sim 8$ GPa a new array of additional peaks appears (Fig. 4, 9.9 GPa). This new structure, designated as the HP phase, coexists with the LP phases and its relative abundance, quantitatively obtained from the GSAS fitting, increases with rising pressure, reaching 100% at ∼10 GPa (see inset of Fig. 5). Three possible structural models suggested in previous studies[15–19] have been considered: the NiAs-type structure (space group $P6_3/mmc$), CdI_2-type (space group $P\bar{3}m1$), and Cr_3S_4-type (space group $I2/m$). Structural refinement analyses assume these three models were carried out using data collected at 15.2 GPa. As can be seen from Table I the diffraction peaks were clearly not consistent with

TABLE I. Parameters characterizing the goodness of fit for different structural models obtained from the GSAS fitting output.

Model	χ^2	w_{Rp}	Rp
NiAs-type	4.765	0.0766	0.0486
CdI_2-type	6.420	0.0889	0.0516
Cr_3S_4-type	0.062	0.0052	0.0036

the NiAs or CdI_2-type structures not to mention the large statistical values of χ^2 (>5), w_{Rp} (>8%), and Rp (>5%). However, for the Cr_3S_4-type structure it was possible to obtain a high-quality fit for all refined patterns (Fig. 4) with $\chi^2 \leqslant 0.07$, $w_{Rp} \leqslant 0.6\%$, and Rp < 0.4%. Hence the Cr_3S_4-type structure (brezinaite) was adopted as the HP phase of $FeCr_2S_4$ (Fig. 6). It is noteworthy that as a result of the spinel → brezinaite structural transition the sulfur sublattice changes from a *fcc* to a *hcp* arrangement; the Cr atoms remain in octahedral sites while the coordination environment of the Fe atoms changes from tetrahedral to octahedral. The positions of the cations are ordered in such a way that alternating layers contain either Fe or Cr.

The complete collection of the diffraction patterns for the pressure range 0–20 GPa was fitted with their respective lattice models: spinel for $P \leqslant 7.5$. GPa and brezinaite for $P \geqslant 10$ GPa and in the coexistence zone a high quality fit could be obtained assuming the presence of these two phases.[27] The resulting graph of lattice parameters and of $V/Z(P)$ (molar volume per $FeCr_2S_4$ unit) are displayed in Fig. 5 (upper portion, 1) and (lower portion, 2). The pressure dependence of the lattice parameters is rather linear below 7.5 and above 11 GPa. Above 7.5 GPa the lattice parameter a of the spinel phase shows an appreciable decrease. Lattice parameters b and c of the brezinaite also demonstrate similar behaviors up to 11 GPa. In the spinel phase range 0.0001–7.5 GPa, data for the molar

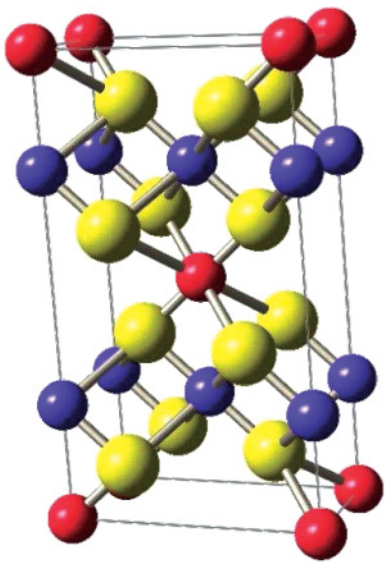

FIG. 6. (Color online) The unit cell of the brezinaite (Cr_3S_4-like) structure for $FeCr_2S_4$ at high pressures. Red, blue, and yellow represent Fe, Cr, and S, respectively. Both Fe and Cr atoms are in octahedral sites.

volume were fitted using the second order Birch-Murnaghan equation of state (EOS)[28]:

$$P = 1.5K_0[(V_0/V)^{7/3} - (V_0/V)^{5/3}], \quad (1)$$

where K_0 and V_0 are the bulk modulus and the unit cell volume, respectively, at room pressure. The fit results in $K_0 = 85.4(6)$ GPa and $V_0/Z = 124.85(4)$ Å^3. Above 7.5 GPa the crystal volume of the spinel phase exhibits an appreciable decrease deviating from the Birch-Murnaghan EOS. The transition to the brezinaite phase is accompanied by an additional discontinuous $\Delta V/V \sim -12\%$ volume change.

3. *Mössbauer studies*

The landscape of the emerging electronic/magnetic phases evolving with pressure can be followed by the MS(P) spectra (Fig. 7) recorded at $T \leqslant T_N$ and up to 20 GPa. Up to ~5 GPa [Figs. 7(a–c)] within the spinel phase and designated as LP1, the spectra are characterized by a single-component magnetically split sextet and a small quadrupole splitting in agreement with previous publications (Ref. 29 and references therein).

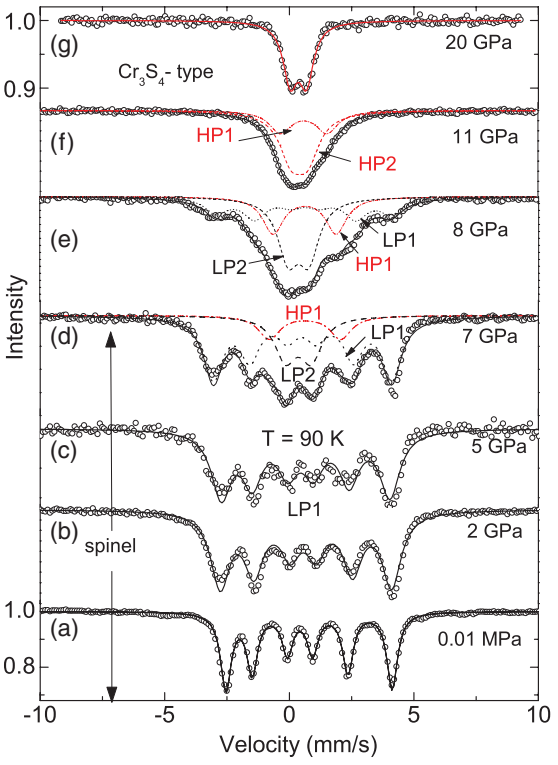

FIG. 7. (Color online) Pressure evolution during compression of the Mössbauer spectra recorded at 90 K ($\ll T_N$), depicting the pressure-induced electronic phases. (a)–(c) Spectra associated with the LP1 phase. (d) At 7 GPa, two new nonmagnetic components appear designated as LP2, with substantially lower IS value and HP1 characterized by a high QS value, respectively. (e) At 8 GPa, the relative abundances of the LP2 and HP1 phases increase at the expense of the LP1. (f) At 11 GPa, LP1 and LP2 both disappear and a new HP2 component emerges. (g) Above 12 GPa, HP2 becomes the only remaining component. The lines through the experimental points are theoretical curves obtained from the least-squares fitting programs.

At 7 and 8 GPa within the coexistence zone, the spectra shown in Figs. 7(d) and 7(e) are the superposition of three components: (1) the magnetically ordered LP1 phase with $H_{hf} = 23$ T [slightly higher than H_{hf} (5 GPa)], QS = 0.05 mm/s, and IS = 0.55 mm/s; (2) a nonmagnetic component designated as LP2 with QS = 0.4 mm/s and IS = 0.3 mm/s, and a second nonmagnetically split component designated as HP1 with QS = 1.2 mm/s and IS = 0.62 mm/s.

From the absence of H_{hf} and from the particular sharp decrease in IS we conclude that LP2, a pressure-induced sequel of the high-spin spinel phase reflects the partial onset of a noncorrelated system typified by the discontinuous decrease in IS and $\langle S \rangle = 0$. Also, we conclude that Fe^{2+} in the HP1 phase, characterized by its large QS and an IS well within the range of values of high-spin ferrous compounds[30] is paramagnetic, belonging to the Cr_3S_4-type phase. At 11 GPa [Fig. 7(f)] the LP components vanish accompanied by the onset of a new, nonmagnetic doublet component, designated as HP2 characterized by QS = 0.3 mm/s and IS = 0.4 mm/s. Low-temperature measurements performed at 20 GPa show the absence of magnetic ordering of HP2 down to 5 K. This and the sharp decrease in QS and IS suggest the onset of a Mott transition in the Cr_3S_4-type phase. At $P > 12$ GPa [Fig. 7(g)], the only spectral component remaining is the HP2 phase.

The pressure dependencies of the QS and IS of the various components are depicted in Figs. 8(b), 8(c), and their relative abundances are depicted in Fig. 8(a). $QS = e^2 q_{zz} QS/2$, where

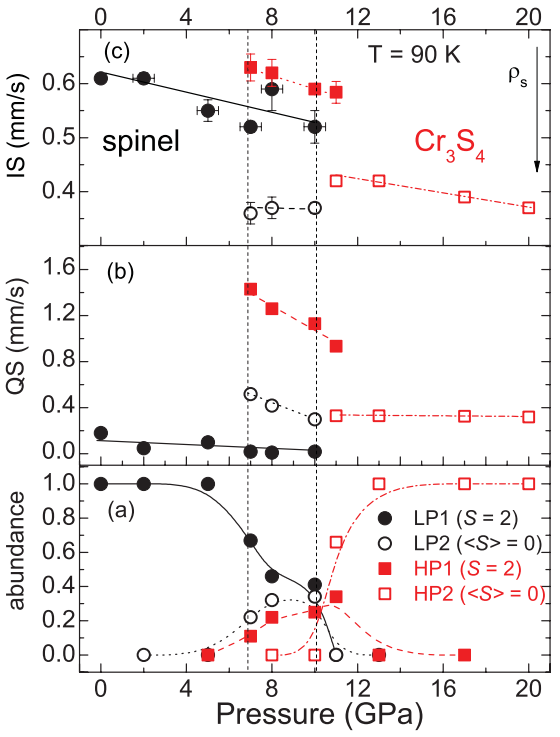

FIG. 8. (Color online) (a) The pressure evolution of the relative abundance of the MS components as computed from the relative values of the absorption areas (see the text). (b) Pressure dependence of the quadrupole splitting at 90 K. (c) Pressure dependence of the IS at 90 K. Note the abrupt decrease in its value at the onset of the LP2 (○) and HP2 (□) phases at 7 and 11 GPa, respectively. Lines are guides to the eyes.

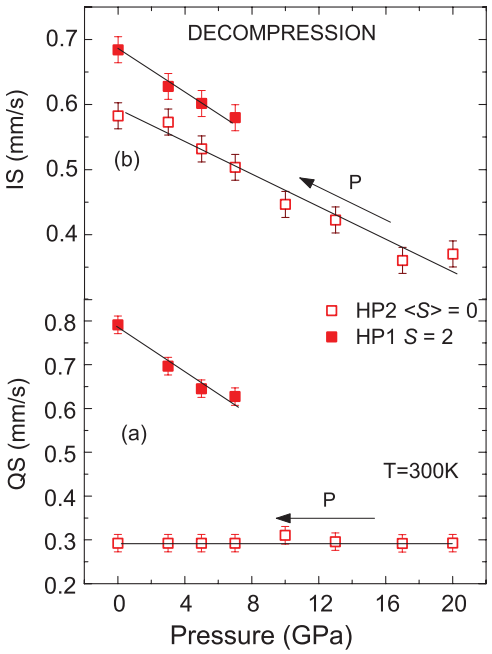

FIG. 9. (Color online) The pressure evolution of the MS parameters at decompression measured at 300 K. (a) Pressure dependence of the quadrupole splitting. (b) Pressure dependence of the IS. Lines are guides to the eyes.

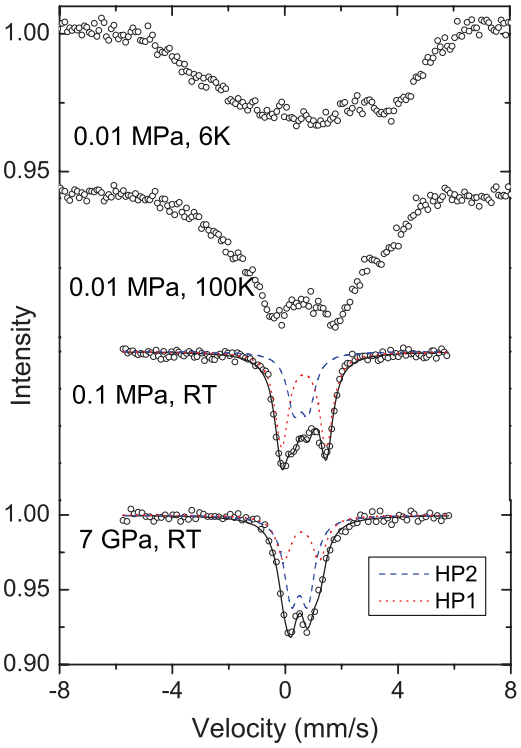

FIG. 10. (Color online) Mössbauer spectra collected at RT during the decompression from 7 GPa to ambient pressure. The lines through the experimental points are theoretical curves obtained from the least-squares fitting programs. The dashed and dotted lines represent the HP2 and HP1 phases, respectively. The relative abundance of HP1 is ~36% at 7 GPa and ~64% at ambient pressure. The broad spectrum at 100 K and the unresolved magnetic splitting at 6 K, recorded at ambient pressure, are indications of a paramagnetic relaxation phenomenon.

eq_{zz} is the electric field gradient and IS is with respect to the ^{57}Co(Rh) source. The relative abundance of site i was determined from the respective areas A_i under the absorption peaks for each component using the relation $A_i = K n_i f_i$, where K is a constant, n_i is the abundance of component i, and f_i is its recoil-free fraction.[31]

Distinctive of the IS(P) curves (Fig. 8) is their monotonous decrease with pressure increase, an upshot of the monotonous increase in $\rho_s(0)$ at the Fe site.[32] The discontinuous decreases at the LP1 → LP2 and HP1 → HP2 are attributed to the decrease in the ferrous-ion radius due to loss of correlation. The QS(P) of LP1 barely changes with pressure, indicating the sturdiness of the Fe^{2+}-O tetrahedral toward distortion. Its small value can be attributed to the rather high symmetric Fe-O_4 tetrahedra. Upon the LP → HP transition followed by an increase in Fe coordination from 4 to 6 one notices a large increase in QS, namely, an electric field gradient typical for high-spin Fe^{2+}-O_6 octahedra. Upon metallization QS drops significantly, which can be attributed to the onset of the d-electrons delocalization and hence, increase in the O_h symmetry.

B. Decompression cycle

1. X-ray diffraction

At decompression down to ambient pressure the sample is composed solely of the Cr_3S_4-type brezinaite phase. The $V(P)$ curve is shown in Fig. 5 (lower portion, 2). As can be seen the compressed/decompressed data coincide along the 10–20 GPa. However the combined compression/decompression $V(P)$ data for the brezinaite phase could not be satisfactorily fitted with a single EOS for the entire 0–20 GPa range. Poor quality fitting, particularly in the 5–13 GPa range, was clearly detected. Satisfactory second-order Birch-Murnaghan fits could be obtained by avoiding the coexistence zone, namely, by fitting the 0.0001–8 GPa and 11–20 GPa ranges separately. The analyses resulted in $K_0 = 43.6(2.1)$ GPa, $V_0/Z = 115.53(47)$ Å^3 and $K_0 = 53.7(1.1)$ GPa, $V_0/Z = 110.89(32)$ Å^3 for the 0–8 GPa and 11–20 GPa ranges, respectively. As can be seen, within the error bars the values of both K_0 and V_0 are definitely different. The elastic constants of these two pressure regimes of brezinaite phase will be clarified with the MS studies.

2. Mössbauer studies

Mössbauer spectra obtained at 300 K with reducing pressure show a significant hysteresis showing that the observed pressure-induced LP-HP phase transition is nonreversible. During decompression the HP2 phase is the only phase observed down to 10 GPa. A new phase is observed at ~7 GPa with IS = 0.58(2) mm/s, QS = 0.63(1) mm/s ($T \approx 300$ K) with 36% abundance, and remains a mixed state with the HP2 phase down to ambient pressure (Figs. 9, 10). The jump in QS and its strong P-dependence and the larger IS suggests the partial recovery of the brezinaite HS state phase assigned as HP1. The paramagnetic features of the HP1 phase

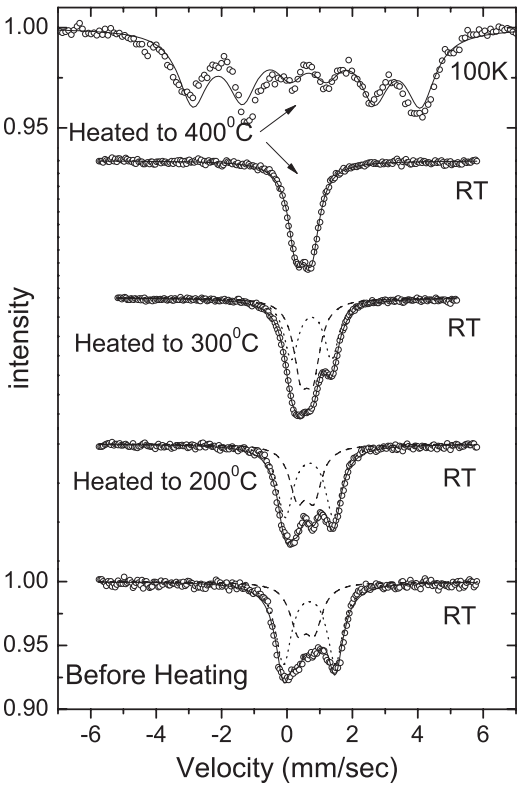

FIG. 11. Mössbauer spectra collected at RT and 100 K after heat treating the sample at various temperatures, 200–400 °C. The lines through the experimental points are theoretical curves obtained from the least-squares fitting programs. The dashed and dotted lines represent the HP2 and HP1 phases, respectively. There is an increase in the relative abundance of HP2 phase when heat treated to 300 °C. A transition to the LP1 takes place only after heat treatment at 400°C.

are revealed (Fig. 10) upon lowering the temperature to $T \leqslant 100$ K.[33]

3. The ambient pressure/temperature stability of the brezinaite phase

To test the brezinaite phase stability at ambient pressure the decompressed sample was heat-treated at various temperatures, and MS spectrum were recorded. During the heating process the pressure was kept at ∼1 GPa to prevent any leakage of air into the sample cavity to eliminate any possibility of oxidation. Each treatment was for a period of 24h. The spectra are shown in Fig. 11. One can see that only after the heat-treatment at $T \approx 400$ °C is a single-site spectrum at RT observed with IS = 0.54(1) mm/s, QS = 0.11(1) mm/s, and a full magnetic splitting at 100 K. This indicates the full spinel recovery.[34]

IV. DISCUSSION

A. The spinel phase

$FeCr_2S_4$ has two distinct electrical transport activation energies: one for the ferrimagnetic phase and the other for the paramagnetic phase [Fig. 2(b)]. According to Wang *et al.*[7] the conductivity of $FeCr_2S_4$ at the high temperature range is dominated by hopping of localized magnetic polarons and the conductivity at the low-temperature range by thermal-activated hopping of carriers. Our data are consistent with such a suggestion and show that these two activation energies decrease linearly with pressure, with two different slopes; the same behavior demonstrates the difference $(E_p - E_f)$. This feature may explain the fact that the resistance peak flattens with pressure: If the peak is the result of a mismatch between the resistance curves at $T > T_N$ and $T \leqslant T_N$, it is easy to understand that with the decrease of $(E_p - E_f)$ the mismatch decreases, and the peak flattens.

We compare our experimental results with recent electrical transport measurements on $FeCr_2S_4$ crystals doped with Cu^{+1} on the Fe site, $Fe_{1-x}Cu_xCr_2S_4$ ($x \leqslant 0.5$).[35] In the latter case the character of the observed effect changes very much in the same manner as in the present study: similar to pressure, doping shifts the Néel temperature and, correspondingly, the resistance peak upwards, accompanied by a decreasing of the CMR effect. There is nonetheless an important difference: the same change of the lattice parameters corresponding to both effects gives a rather different shift of the resistance maximum. Thus applying a pressure of 6 GPa and doping by 27% of Cu^{+1} both produce quite similar ∼0.3% shrinkage of the lattice parameter, but the resistance maximum shifts are correspondingly ∼25 and 60 K. A comparatively weaker effect of pressure application (in terms of parameter shrinkage) on T_N could be rationalized by taking into account some additional aspects of the doping, namely, (i) Cu^{+1} is a nonmagnetic impurity and (ii) Fe valence changes to +3.[36] By contrast, application of pressure affects mainly the band width and gives rise to a gap closure.

With a pressure increase to ∼7 GPa, an insulator-to-metal transition takes place which corroborates with the collapse of Fe^{2+} magnetic moments. Concurrency of both transitions prompted us to conclude that the breakdown of the *d*-*d* electronic correlation due to the Mott transition is responsible for the observed transformation. A consequence of the MT is the collapse of the CMR effect due to the collapse of magnetism. Another experimental result is that the electronic and crystallographic transitions start at almost the same pressure, which strongly suggests that the two transitions are related to each other. There is a simple interpertation: the delocalized state of some electrons and Fe^{2+} diamagnetic state is a property of the band structure of the brezinaite lattice. In other words, the transition to a metallic and nonmagnetic state is a direct outcome of the crystallographic transition. But this suggestion contradicts some experimental results, namely:

(1) A primary metallic behavior is already observed at 7 GPa, below the first appearance of the brezinaite phase (8 GPa) and further below the pressure at which the abundance of this phase crosses the percolation threshold (∼30–40%). Furthermore, by close examination of Fig. 2(b) one notices that according to the trend of the $E_f(P)$ curve, the band gap is expected to vanish at 9.7 GPa, not far from the pressure that the transition to metallic state actually took place. This feature implies that the transition to the metallic state is due to the closure of the gap—due to the Mott transition.[8,9] Usually in Mott transitions there is a free-energy instability when the intra-atomic correlation energy is comparable to the bandwidth

($U \sim W$), which results in a phase separation to metallic and insulating phases even when the gap is still finite.[8] Hence an electronic transition at 7 GPa is not at all surprising.

(2) The lattice parameters and crystal volume of the spinel phase (Fig. 5) shows no monotonic behavior above 7.5 GPa: the lattice parameter and the volume exhibit an appreciable decrease. This is consistent with the abrupt decrease in IS (Fig. 8), i.e., increase in $\rho_s(0)$ in the LP2 phase. Since this structural transformation is in accordance with the onset of the IM transition and appearance of the nonmagnetic LP2 phase, we attribute it to the consequential structural alteration of the MT. This is undoubtedly the best evidence that the appearance of the metallic and nonmagnetic state (LP2 phase) is caused not by the crystallographic transition to the brezinaite phase but by the electronic transition in the spinel phase.

It is known that an electronic transition could be accompanied by some alteration of structural parameters and corresponding isostructural transition (e.g., Ref. 11), and that is what happens in the $FeCr_2S_4$ spinel phase. But why is this electronic transition further accompanied by a fundamental structural transformation and symmetry change? The total free energy of a certain solid phase can be split into the ground state contribution of the static lattice F_{sl} and into additional contributions for the various types of excitations: $F = F_{sl} + F_{ph} + F_{el}$, where F_{ph} represents the free energy of phonons, F_{el} is the free energy of the conduction electrons and all the other possible excitations like magnons and lattice defects. In the calculation of the free energy of possible crystallographic phases it is usually assumed that $F_{sl} > F_{ph}, F_{el}$, so the two last terms may be neglected. However this assumption is not always valid. We have noticed that the brezinaite phase could be preserved down to ambient pressure. The fact that both phases, spinel and brezinaite, can exist in the same pressure range is an indication of the small difference between their free energies, and in such a case the contributions of the terms F_{ph} and F_{el} become appreciable. Another confirmation of a proximity of the free energies of both structures is the fact that in a series of ternary chromium sulfides ACr_2S_4, where A is a divalent transition metal, both structures are realized at ambient conditions (spinel for $A =$ Mn, Fe, Co[37] and brezinaite for $A =$ V, Ti, Cr, Ni[38]).

The reason for the realization of both structures can be attributed to the competition between two contradicting tendencies. On one hand the brezinaite structure is less stable than the spinel because the first has face-sharing octahedrons, whereas the second has only-edge sharing octahedrons that keep the positively charged cations further apart (e.g., Ref. 39, p. 234). On the other hand, the crystal-field stabilization energy due to the interaction between the $3d$ electrons of the cation and the $3p$ and $3s$ electrons of the surrounding anions is usually higher for octahedral than it is for tetrahedral sites (e.g., Ref. 40, p. 105). In the spinel structure Fe^{2+} ions are in tetrahedral sites, whereas in the brezinaite structure they are in octahedral sites. As a result the latter structure has higher crystal-field stabilization energy. It is known that the preference for octahedral sites is higher for V^{2+}, Ti^{2+}, Cr^{2+}, and Ni^{2+} than for Mn^{2+}, Fe^{2+}, and Co^{2+},[41] thus, it seems that only for the first four the stabilization energy is large enough to overcome the destabilizing effect of face-sharing octahedrons. The previous consideration undoubtedly suggests that for this group of materials the two contradicting stabilization effects have comparable energies, and the balance between the two effects might be tipped by relatively small perturbations, such as F_{el}. The change in F_{el} due to the gap closures of the Mott-Hubbard (MH) intraband or the Charge-Transfer (CT) interband may be just enough for triggering this structural phase transition.

B. The brezinaite phase

The pressure-induced MT in $FeCr_2S_4$ is further accompanied by a first-order structural transformation from spinel to the Cr_3S_4-type structure. According to the Mössbauer data two phases are associated with this structure: HP1 and HP2. The first one is paramagnetic and the HP2 phase is nonmagnetic. Thus we can conclude that a regaining of magnetic moment by Fe ions occurs at the LP $\rightarrow$ HP1 transition followed by their recurring loss at the transition to the HP2 phase. The latter could be either due to a high spin–low spin transition or breakdown of the d-d electronic correlation due to a Mott transition, which in contrast to a HS-LS transition, will be intrinsically accompanied by metallization. The fact that up to 10 GPa the material shows a pure metallic behavior supports the latter mechanism. Similar to the spinel case, this electronic transition corroborates with an appreciable volume drop ($\sim$2%) within the 8–11 GPa pressure range (Fig. 5).

An important feature obtained from the XRD experiment is the significant decrease of the bulk modulus following the transition to the HP phase. This feature is quite typical for the spinels: our recent studies of a series of ferrite spinels MFe_2O_4 ($M =$ Mg, Co, Zn, Fe) have shown the same feature.[42]

V. CONCLUSIONS

In conclusion the observed series of intertwined structural, electronic, and magnetic changes in $FeCr_2S_4$ include the onset of Mott transition in the LP spinel phase. This electronic transition initiates structural instability of the spinel structure resulting in the nonreversible structural transition to a Cr_3S_4-like HP structure at the 8–10 GPa pressure range. The onset of the HP phase is accompanied by the Fe 4–6 coordination number increase and $\sim$12% volume reduction. Beyond 10 GPa the isostructural correlated $\rightarrow$ noncorrelated transition takes place to nonmagnetic Fe^{2+}. Under decompression the HP phase undergoes a recovering of its localization features with no appreciable hysteresis in pressure. It is noteworthy that the trend toward gap closure observed in the spinel phase preceding the Mott transition corroborates with the suppression of the $R_{\max}(P)$, corresponding to the CMR effect.

ACKNOWLEDGMENT

This research was supported in part by the Israeli Science Foundation Grants #36/05 and #789/10. We acknowledge the European Synchrotron Radiation Facility for provision of synchrotron radiation facilities beam line ID09. The DACs were provided in kind by D'Anvils Ltd. (www.danvils.com)

*moshepa@post.tau.ac.il

[1] F. K. Lotgering, Phillips Res. Rep. **11**, 190 (1956).

[2] P. F. Bongers, C. Haas, A. M. J. G. Van Run, and G. Zanmarchi, J. Appl. Phys. **40**, 958 (1969).

[3] A. P. Ramirez, R. J. Cava, and J. Krajewski, Nature **386**, 156 (1997).

[4] A. P. Ramirez, J. Phys. Condens. Matter **9**, 8171 (1997); J. M. D. Coey, M. Viret, and S. Von Molnár, Adv. Phys. **48**, 167 (1999); Y. Tokura and Y. Tomioka, J. Mag. Mag. Mater. **200**, 1 (1999); M. B. Salamon and M. Jaime, Rev. Mod. Phys. **73**, 583 (2001).

[5] H. M. Palmer and C. Greaves, J. Mater. Chem. **9**, 637 (1999).

[6] M. S. Park, S. K. Kwon, S. J. Youn, and B. I. Min, Phys. Rev. B **59**, 10018 (1999).

[7] S. Wang, K. Li, Z. Chen, and Y. Zhang, Phys. Rev. B **61**, 575 (2000).

[8] N. F. Mott, *Metal-Insulator Transitions*, (Taylor & Francis Ltd., London, 1974).

[9] M. Imada, A. Fujimori, and Y. Tokura, Rev. Mod. Phys. **70**, 1039 (1998).

[10] V. Tsurkan, I. Fita, M. Baran, R. Puzniak, D. Samusi, R. Szymczak, S. Kimm, M. Klemm, S. Horn, and R. Tidecks, J. Appl. Phys. **90**, 875 (2001).

[11] G. Kh. Rozenberg and M. P. Pasternak, Phase Transitions **80**, 1131 (2007); G. Kh. Rozenberg, M. P. Pasternak, W. M. Xu, L. S. Dubrovinsky, and M. Hanfland, High Press. Res. **30**, 238 (2010).

[12] J. P. Rueff, C. C. Kao, V. V. Struzhkin, J. Badro, J. Shu, R. J. Hemley, and H. K. Mao, Phys. Rev. Lett. **82**, 3284 (1999).

[13] D. Lundqvist, Ark. Kemi. Min. Geol. **17B**, 12 (1943).

[14] Z. Chen, S. Tan, Z. Yang, and Y. Zhang, Phys. Rev. B **59**, 11172 (1999).

[15] W. Albers and C. J. M. Rooymans, Solid State Comm. **3**, 417 (1965).

[16] R. J. Bouchard, Mat. Res. Bull. **2**, 459 (1967).

[17] Recent studies of materials with the Cr_3S_4-like structure revealed that at high temperatures a transition to a CdI_2-like structure ($P\bar{3}m1$) takes place, see Y. Oka, K. Kosuge, and S. Kachi, Mat. Res. Bull. **15**, 521 (1980); J. Solid State Chem. **24**, 41 (1978); T. Ohtani, R. Fujimoto, H. Yoshinaga, and M. Nakahira, *ibid.* **48**, 161 (1982).

[18] Oka Kosuge and S. Kachi, J. Solid State Chem. **24**, 41 (1978); T. Ohtani, R. Fujimoto, H. Yoshinaga, and M. Nakahira, *ibid.* **48**, 161 (1982).

[19] P. Vaqueiro, A. V. Powell, S. Hull, and D. A. Keen, Phys. Rev. B **63**, 064106 (2001).

[20] E. Sterer, M. P. Pasternak, and R. D. Taylor, Rev. Sci. Instrum. **61**, 1117 (1990).

[21] A. P. Hammersley, *FIT2D: An Introduction and Overview*, ESRF Internal Report, ESRF97HA02T (1997).

[22] A. P. Hammersley, S. O. Svensson, M. Hanfland, A. N. Fitch, and D. Hausermann, High Press. Res. **14**, 235 (1996).

[23] A. C. Larson and R. B. Von Dreele, *General Structure Analysis System (GSAS)*, LANL Report LAUR 86-748 (2000).

[24] B. H. Toby, J. Appl. Crystallogr. **34**, 210 (2001).

[25] G. K. Rozenberg, G. R. Hearne, M. P. Pasternak, P. A. Metcalf, and J. M. Honig, Phys. Rev. B **53**, 6482 (1996).

[26] Z. Yang, S. Tan, Z. Chen, and Y. Zhang, Phys. Rev. B **62**, 13872 (2000).

[27] At the coexistence zone one may expect that patterns of the LP and HP phases will be composed of a superposition of the LP1 + LP2 and HP1 + HP2 phases, respectively. However because a typical line width of the patterns significantly exceeds the splitting associated with the difference in the lattice parameters of the above mentioned phases, a composite diffraction pattern will not be split but become asymmetrically broadened compared to the pattern of a single phase. Indeed, the line width of the brezinaite (002) peak is 11% larger at the 8–10 GPa range as compared to pressures above 10 GPa. Also, the Cagliotti's Gaussian term V; the GV profile parameter in the GSAS refinement shows a ∼2× increase at the 8–10 GPa range. A similar situation arises in the LP1–LP2 coexistence.

[28] O. L. Anderson, *Equations of State of Solids for Geophysics and Ceramic Science*, (Oxford University Press, New York, 1995).

[29] Z. Klencsár, E. Kuzmann, Z. Homonnay, A. Vértes, A. Simopoulos, E. Devlin, and G. Kallias, J. Phys. Chem. Solids. **64**, 325(2003).

[30] IS values of high-spin ferrous compounds ($S = 2$) at ambient pressure are usually within the range of 0.7–1.5 mm/s, meanwhile in the case of $\langle S \rangle = 0$ IS values are within the range of −0.25–0.35 mm/s (see N. N. Greenwood and T. C. Gibb, *Mossbauer Spectroscopy*, (Chapman and Hall Ltd., London, 1971) and references therein).

[31] We assumed as a first approximation that at each pressure the recoil-free fraction values f_i for the three components are the same at 90 K.

[32] $IS(Fe^{57}) \propto \rho_s(0) \cdot \Delta R/R$, where $\rho_s(0)$ is the s-electron density at the Fe-nucleus and $\Delta R/R$ is the relative difference between the nuclear radii of the excited and ground states.

[33] The spectral-line broadening is due to paramagnetic relaxation superimposed with the quadrupole split spectrum of HP2. See W. M. Xu, O. Naaman, G. Kh. Rozenberg, M. P. Pasternak, and R. D. Taylor, Phys. Rev. B **64**, 094411 (2001).

[34] Indeed, a measurement of the pressure after heating at 400 °C shows a pressure increase to ∼3 GPa. This increase during heating is an unusual phenomenon since usually when a pressure cell is heated the pressure in it decreases due to a thermal expansion of the screws. The explanation for this increase in pressure is probably related to a significant increase in the unit cell volume during the crystallographic transition to the spinel structure. The spectral-line broadening is due to paramagnetic relaxation superimposed with the quadrupole split spectrum of HP2.

[35] V. Fritsch, J. Deisenhofer, R. Fichtl, J. Hemberger, H.-A. Krug von Nidda, M. Mücksch, M. Nicklas, D. Samusi, J. D. Thompson, R. Tidecks, V. Tsurkan, and A. Loidl, Phys. Rev. B **67**, 144419 (2003).

[36] G. Haacke and A. J. Noizik, Solid State Commun. **6**, 363 (1968).

[37] H. Hahn, Z. Anorg. Chem. **264**, 184 (1951).

[38] C. N. R. Rao and K. P. R. Pisharody, Prog. Solid State Chem. **10**, 207 (1979).

[39] W. Borchardt-Ott, *Crystallography*, (Springer, Berlin, Heidelberg, New York, 1995).

[40] A. R. West, *Basic Solid State Chemistry*, (John Wiley & Sons, Chichester, 1999).

[41] A. Miller, J. Appl. Phys. **30**, 24S (1959).

[42] W. M. Xu, E. Greenberg, G. Kh. Rozenberg, M. P. Pasternak, L. S. Dubrovinsky, and G. Garbarino (to be submitted for publication).

[43] W. I. F. David, J. Res. Natl. Inst. Stand. Technol. **109**, 107 (2004).